

H₂ AND Br γ NARROW-BAND IMAGING OF BIPOLAR PLANETARY NEBULAE.M. A. GUERRERO¹, E. VILLAVER

Instituto de Astrofísica de Canarias, E-38200 La Laguna (Tenerife), Spain

A. MANCHADO

Instituto de Astrofísica de Canarias, E-38200 La Laguna (Tenerife), Spain

Consejo Superior de Investigaciones Científicas, CSIC

P. GARCÍA-LARIO

ISO Data Centre, Estación de Villafranca del Castillo, Apdo. Postal 50727, E-28080 Madrid, Spain

F. PRADA²

Instituto de Astrofísica de Canarias, E-38200 La Laguna (Tenerife), Spain

To appear in The Astrophysical Journal Supplement Series

ABSTRACT

We present near-IR narrow-band continuum-subtracted images in the H₂ 2.122 μ m, and Br γ 2.166 μ m emission lines for a sample of 15 bipolar planetary nebulae. H₂ emission was definitely detected for most of the objects in this sample (13 out of 15). The very high H₂ detection rate supports the idea that bipolar planetary nebulae have important reservoirs of molecular material and offer suitable physical conditions for the excitation of H₂. The strength of the H₂ emission and the H₂/Br γ flux ratio are found to correlate with the morphology of the bipolar nebulae observed. Bipolar PNe with broad and bright rings exhibit stronger H₂ emission than bipolar PNe with narrow twists. High-quality (sub-arcsec) [N II] and H α optical images have been used to compare the distribution of the ionized and molecular material. The H₂ emission lies just outside the optical [N II] emission zone.

Subject headings: infrared: interstellar medium: lines and bands – interstellar medium: molecules – planetary nebulae: general

1. INTRODUCTION

Planetary Nebulae (PNe) form when low- and intermediate-mass ($< 10 M_{\odot}$) stars evolve off the asymptotic giant branch (AGB) phase to white dwarfs. In this short-lived transition, AGB stars eject most of their envelope which become thick circumstellar shells. The central star will later ionize this material and a new PN arises. While the visible PN is dominated by ionized gas, molecular material may still survive in high-density clumps or in the photo-dissociation region (PDR) where the optical depth to ionizing photons is high (Tielens 1993). The presence of residual molecular gas in PNe, remnant of the AGB envelope, provides us with important hints about the mass-loss history and geometry on and at the end of the AGB, and offers some insight into the formation mechanism of PNe.

Extensive surveys in the CO (2–1) line in PNe (Huggins & Healy 1989; Huggins et al. 1996, and references therein) have shown that molecular envelopes are widely observable in PNe and constitute a significant component of their masses. The large format near-IR arrays avail-

able nowadays make the observations in the H₂ 2.122 μ m emission line (hereinafter we will refer to this line as H₂, except when explicitly indicated) a powerful tool for the study of the distribution of molecular gas in PNe. Since the first detection of this line in the young PN NGC 7027 (Treffers et al. 1976), over 60 other PNe and proto-PNe have been detected in this line (Webster et al. 1988; Zuckerman & Gatley 1988; Kastner et al. 1994, 1996, and references therein; Hora & Latter 1996), and the number of detections is increasing steadily. Some doubts about the validity of the H₂ emission line as a quantitative probe of the total molecular mass have been posed (*e. g.* Dinerstein 1991) as this line can be excited either by fluorescence through the absorption of UV photons from the central star in the photo-dissociation front (Black & van Dishoeck 1987; Sternberg & Dalgarno 1989) or by shocks (*e. g.* Burton, Hollenbach, & Tielens 1992). The comparison between CO and H₂ emission in PNe (Huggins & Healy 1989; Huggins et al. 1996) shows that the H₂ emission is indeed related to the amount of molecular gas in

¹Currently at Department of Astronomy, University of Illinois at Urbana-Champaign, 1002 West Green Street, Urbana, IL 61801²Currently at Centro Astronómico Hispano-Aleman, Apdo 511, E-04080, Almería, Spain

PNe.

The CO and H₂ observations of PNe have revealed that molecular gas is predominantly detected in bipolar PNe, although emission is also found among other morphological classes. Bipolar PNe have relatively dense equatorial regions which provide a safe haven for molecules due to self- and dust-shielding of UV photons. They are also associated to high-mass progenitor stars (Peimbert & Torres-Peimbert 1983; Zuckerman & Gatley 1988; Corradi & Schwarz 1995; Huggins et al. 1996) which presumably have experienced higher mass ejections.

The bipolar PN class is not homogeneous as a whole, as two distinct types of detailed morphologies exist (Manchado et al. 1996, hereafter M96; Manchado 1997): (1) bipolar PNe with a compact core or narrow waist (class B); (2) bipolar PNe with a broad ring structure in the waist (class Br). Balick (1987) already noticed this morphological difference (the so-called early and late butterfly types) and proposed that B PNe evolve into Br PNe.

Webster et al. (1988) reported observations of a sample of 11 bipolar PNe and noted that Br PNe have the highest H₂ intensity and H₂ to Br γ flux ratio. However, their results should be used with caution due to poor spatial resolution ($\sim 5'' \times 14''$) and sampling. The latter tends to maximize the H₂ to Br γ flux ratio. This can be seen in some individual objects, as NGC 7027, whose flux ratio, as given by Webster et al., does not account for the H₂ to Br γ large ratio variations over the nebula (Cox et al. 1997).

In order to gain more insight into the correlation between H₂ emission and the detailed morphology of bipolar PNe, this paper presents near-IR narrow-band images in the H₂ and Br γ lines of a sample of 15 bipolar B and Br PNe selected from the narrow-band images displayed by M96. The H₂ and Br γ fluxes of these PNe have been measured and accurate H₂ intensities and H₂ to Br γ flux ratios of each subgroup of bipolar PNe have been obtained. The results are compared with these previously presented by Webster et al. (1988) and the implications on the formation and evolution of bipolar PNe are discussed. Moreover, the comparison of the H₂ and optical images from the M96 catalog have been used to analyze the relative distribution of ionized and molecular material. Finally, a detailed description of the individual morphology of some peculiar PNe in the sample is given.

2. OBSERVATIONS

2.1. Sample selection criteria

The nebulae were selected according to the following criteria:

1. All the nebulae are bipolar or quadrupolar PNe, showing a 'waist' and (at least) two bipolar lobes.
2. They have dereddened H β fluxes in the range $3.2 \cdot 10^{-13} \leq F(H\beta) \leq 5.1 \cdot 10^{-11}$ erg cm $^{-2}$ s $^{-1}$, and

[N II] morphologies indicative of the presence of dense low-ionization equatorial regions.

3. They have angular sizes larger than $15''$ to resolve them properly, and smaller than $150''$ to make them fit into the field of view.

2.2. Data acquisition

Near-IR images of the selected fields were obtained on 24 and 25 June 1996 with the MPI für Astronomie General-Purpose Infrared Camera (MAGIC) attached to the f/8 Cassegrain focus of the Calar Alto (CAHA) 2.2m telescope. The detector was a Rockwell 256 \times 256 pixel² NICMOS3 array. The high resolution imaging mode was used with a pixel scale of $0.64''$ pixel $^{-1}$, and a field of view of $164''$. The filter parameters are described in Table 1.

Different observing strategies were followed for compact and extended sources. Compact sources were observed rastering them to different locations of the detector, so that the image resulting from the combination of different frames before centering can be used as a sky frame. In the case of extended sources, adjacent blank sky regions observed between consecutive on-source exposures were combined to obtain the corresponding sky frame. In both cases, the integration time on the object was always 100 sec. The images presented here are composed of many shorter exposures which were then individually sky-subtracted and flat-fielded before centering and averaging them to produce the final images. The FWHM of point sources in the final images, which includes both the seeing at $\lambda = 2.2\mu\text{m}$ and instrumental effects, are in the range $1.''1 - 1.''5$. The weather was photometric through the whole observing run. The sensitivity at 3σ over the background was found to be $\sim 3.0 \cdot 10^{-5}$ erg cm $^{-2}$ s $^{-1}$ sr $^{-1}$.

2.3. Data reduction

As opposed to optical emission from PNe, strongly dominated by narrow nebular emission lines, the situation is very different in the near-IR, where the continuum emission sometimes becomes very important and can even dominate the observed emission. Unfortunately, there were no H₂ and Br γ continuum filters available at the telescope. Thus, in order to subtract the continuum emission from the narrow-band images, we obtained additional broad-band K' images.

The subtraction of the continuum emission requires some detailed explanation. First, we scaled the broad- and narrow-band emission using images of the flux standard star SA 107-1006 (Casali & Hawarden 1992) obtained at both filters, assuming that the continuum of this star is roughly constant through the K' -band. Then, for each nebula we subtracted the emission from the H₂ and Br γ to the continuum image of the nebula. Finally, after scaling, we subtracted these non-contaminated by emission lines continuum images to the original H₂ and Br γ images in order to obtain continuum-subtracted images in these lines.

The H₂ and Br γ narrow-band continuum-subtracted images for all the PNe are presented in Figure 1. For comparison, the [N II] optical images from M96 are also presented at the same scale.

The contribution from other emission lines to the flux observed in the K' -band has carefully been considered. Besides Br γ and H₂ 2.122 μm , the most prominent emission lines in this band are Br8 H I, He I 2.058, and a few H₂ emission lines at 1.957, 2.033, 2.223 and 2.248 μm . After re-scaling the continuum image, the expected contribution from Br8 H I and He I 2.058 is estimated to be $\sim 2\%$ the intensity of Br γ , whereas the contribution of the H₂ lines is $\leq 5\%$ the intensity of the H₂ 2.122 μm line.

Similarly, we have analyzed the contribution of the He I 2.1126 μm line to the flux observed in our narrow-band H₂ images. Hora, Latter, & Deutsch (1999) presented reliable measurements of the intensity of the He I 2.1126 μm and Br γ lines for 33 PNe. The average intensity of the He I 2.1126 μm line is $\sim 5\%$ the intensity of the Br γ line. Therefore, a significant contribution from the He I 2.1126 μm line to our narrow-band H₂ images is only expected when Br γ is much more intense than H₂. Even in these cases, the emission in the H₂ and He I lines comes from different regions in the PN, and therefore it is still possible to distinguish between H₂ and He I emission.

The standard star SA 107–1006 was used for flux calibration. The measured H₂ and Br γ fluxes are given in Table 2. Given the inherent high-noise and short-term fluctuations of the near-IR sky background, and the uncertainties above described affecting the continuum subtraction, the measured fluxes can be affected by relative errors which have been estimated to be $\leq 5\%$ for fluxes larger than $1.0 \cdot 10^{-12} \text{ erg cm}^{-2} \text{ s}^{-1}$, and 5–20% for smaller fluxes.

3. DETECTION OF MOLECULAR HYDROGEN

Table 2 lists the usual names³ and approximate galactic coordinates (the PN G name as described by Acker et al. 1992) of the objects observed (columns 1 and 2); the morphological classification (column 3); the angular size of the whole nebula and its ring (columns 4, and 5) in the optical as given by M96; and the dereddened H β fluxes (column 6) as obtained from Acker et al. (1992). Table 2 also summarizes the main results of this work: the measured fluxes in the H₂ and Br γ lines (columns 7 and 8); the H₂ to Br γ flux ratio (column 9); and the H₂ surface brightness ratio between the lobes and the ring (column 10), f_{LR} , defined as

$$f_{\text{LR}} = \frac{B_{\text{lobe}}}{B_{\text{ring}}} \quad (1)$$

where B_{lobe} and B_{ring} is a rough estimate of the peak surface brightness of the lobes and ring, respectively.

³The acronym ‘He’ is used through this work to name Henize’s objects, despite the fact that ‘Hen’ is the acronym used in astronomical dictionaries. The former is used in The Strasbourg-ESO Catalogue of Galactic Planetary Nebulae (Acker et al. 1992) and is widely accepted.

Emission in the H₂ images (Fig. 1) was detected above 3σ level in all but one (He 2-428) of the nebulae in our sample. The possible contamination due to the He I 2.1126 μm line may become relevant only for the objects with the lowest H₂ to Br γ ratios: M 1-57, M 1-59, M 2-46, and He 2-437. In particular, we cannot exclude that the emission detected in M 2-46 is due to He I. The detection of H₂ emission is confirmed in M 1-57, M 1-59, and He 2-437 according to morphological criteria; the H₂ emission is detected in the lobes of those nebulae, where Br γ emission is not detected. In the case of He 2-437, where Br γ emission is detected in the lobes, it should be noted that the position angle of the emission in the H₂ image differs from that in the Br γ image, but it follows the [N II] emission. Since the H₂ fluxes of M 1-59 and M 2-46 given in table 2 correspond to the whole nebulae, these values should be considered as upper limits; the H₂ fluxes of M 1-57 and He 2-437 were measured in the lobes, excluding the central part. Therefore, the emission detected in 13 of the bipolar PNe in our sample is connected with H₂ emission from these nebulae.

Figure 2-[top] shows the dereddened Br γ fluxes plotted against the H β fluxes. Adopting case B recombination, $T_{\text{e}} = 10^4 \text{ K}$ and $N_{\text{e}} = 10^3 \text{ cm}^{-3}$, the theoretical Br γ to H β flux ratio is expected to be ~ 0.03 (Osterbrock 1989). This relation is shown as a dashed straight line in Fig. 2-[top]. Although a correlation between Br γ and H β fluxes is found, most of the objects in our sample fall below the predicted Br γ to H β fluxes ratio; this is probably due to the poor accuracy of the H β flux determination, based for most of the objects on a rough extrapolation from H β flux determination on a small portion of the object (Acker et al. 1991) which is likely underestimating the real H β flux.

The measured H₂ fluxes are plotted against the Br γ fluxes in Fig. 2-[bottom]. It is clear that our sample breaks down into two different locations on this diagram. In agreement with the values of the H₂ to Br γ flux ratios listed in Table 2, we distinguish two well defined subgroups in our sample: those PNe whose H₂ flux is several times (≥ 5) stronger than the Br γ flux, and those in which the Br γ emission clearly dominates. Globally considered, the $F(\text{H}_2)/F(\text{Br}\gamma)$ ratios observed span two orders of magnitude. As we discuss below, these nebulae have different morphological and physical properties.

3.1. H₂ dominated bipolar PNe

We can include BV 1, K 3-34, K 3-58, K 4-55, M 1-75, M 2-52, M 4-14, and M 4-17 in this group. In all these cases the emission observed in the H₂ line is more than 5 times greater than the Br γ emission. The measured H₂ flux is in the range $5 \cdot 10^{-13}$ to $4 \cdot 10^{-12} \text{ erg cm}^{-2} \text{ s}^{-1}$, with peak intensities $1.2 - 5.3 \times 10^{-4} \text{ erg cm}^{-2} \text{ s}^{-1} \text{ sr}^{-1}$.

The morphologies observed in the H₂ line (Fig. 1) closely resemble those shown in the optical [N II] lines (M96). The H₂ emission is mainly concentrated in a bright ring, the “waist” of the bipolar nebula. The peak emission of the ring has a surface brightness more than two times brighter than the projected edge of the lobes, as listed in Table 2. The surface brightness contrast between the ring and lobes is, however, much less extreme than in the optical [N II] $\lambda 6583$ line. In contrast, the much fainter Br γ emission is detected only in the central ring, which appears sharper in the H₂ line than in the Br γ line.

All of these PNe share some common properties. First, all of them exhibit well defined rings in the light of [N II]. Indeed, they all are Br or “quadrupolar” (Q) with ring PNe according to the scheme derived from optical observations proposed by M96. Note that BV 1 can also be included in this group, although its ring is not so evident, as it is seen edge-on (Kaler, Chu, & Jacoby 1988; Josselin et al. 1999). The rings of these PNe are characterized by a high surface brightness contrast between the ring itself and its innermost part. The emission in the [N II] and H₂ lines arises mainly in both cases from the ring, but the center of the ring does not show any emission in these lines or very little. These PNe have also relatively low density (100 to 1000 cm⁻³) (Acker et al. 1992), and the averaged size of their rings is 0.22 pc. In addition, their central stars are all faint to be detected in the optical images with the exception of the very faint central star of M 4-14.

3.2. Br γ dominated bipolar PNe

In contrast with the PNe above cited, the bipolar PNe He 2-437, M 1-57, M 1-59, NGC 6881, and PC 20 are characterized by a small H₂ to Br γ flux ratio ($F(H_2)/F(Br\gamma) \sim 0.1 - 0.5$). All of them show emission in the Br γ line strongly concentrated in the central, bright core. H₂ emission is detected both at the central regions and along the bipolar lobes in most cases, although the H₂ emission is always fainter than the Br γ emission.

He 2-437 and M 1-57 show an unresolved core. They also exhibit the most extremely low H₂ to Br γ flux ratios ($\sim 0.1 - 0.2$), whereas for M 1-59, NGC 6881, and PC 20, the H₂ to Br γ flux ratios increase up to 0.2–0.5. These latter nebulae, classified as Br PNe by M96, have small sized central rings, with a small surface brightness contrast between the innermost part of the ring and its edge in the [N II] line. M 1-59, NGC 6881, and PC 20, therefore, show intermediate properties between the Br γ emission dominated class B PNe with unresolved cores (He 2-437 and M 1-57) and the H₂ emission dominated class Br PNe described above.

The bipolar PNe in this subgroup exhibit different properties than the H₂ dominated bipolar PNe. Their central regions have a high surface brightness, in agreement with their larger densities (10^3 to 10^4 cm⁻³) (Acker et al. 1992). Their averaged size is only 0.076 pc. Finally, many of the

central stars of this subgroup of PNe are very bright in the optical images.

3.3. Comments on individual objects

NGC 6881.

The [N II] image of this nebula (Guerrero & Manchado 1998) shows a highly collimated bipolar structure with a size of $29.5'' \times 5''$. Each lobe ends as a bright knot where the emission in the [N II] light is enhanced. A second, brighter pair of inner lobes extends over $16''$. Finally, a loop-like structure is located $11''$ towards the southeast extreme of the nebula.

The differences between the [N II] and H₂ images of this nebula are obvious. Unlike observed in the optical, a pair of very opened lobes is being collimated by a marked $4''$ waist which roughly corresponds to the ring observed in the optical. The lobes extend $20''$ to the north-west and $13''$ to the south-east, almost coinciding with the south-east loop-like structure. As the lobes separate from the central waist, their width increases to a maximum dimension of $16''$. As it is illustrated in Figure 3, the corresponding width of the optical lobes at this position is less than $5''$. Beyond the limit of the northwest lobe, but at the same position angle, extended emission is found as a continuation of this lobe. The maximum angular distance at which we found emission is $\sim 50''$, almost twice the angular dimension of the ionized emission. NGC 6881 is also a member of the group of peculiar PNe whose H₂ morphology does not trace the ionized emission, as it is the case of J 900 (Shupe et al. 1995) and NGC 2440 (Latter et al. 1995; Latter & Hora 1997).

M 1-57

H₂ emission is marginally detected $\sim 30''$ from the centre of the nebula with the same orientation of the $15''$ sized optical lobes (M96). Deeper images, both in the [N II] and H₂ lines, are needed to confirm this result.

He 2-428.

This is the only bipolar PNe not detected in the H₂ line. It is an intriguing situation, since it belongs to the Br class of M96 and it is similar in many aspects to other nebulae in this group, whose H₂ flux is a few times stronger than the Br γ emission. However, while Br γ emission is detected in He 2-428, the nebula is not detected in H₂. In addition, this is the only case of a nebula in our sample in which a bright central star is found. Since the central stars of nebulae with bright H₂ emission in our sample are very faint and difficult to detect, it is urged to investigate in detail the nature of He 2-428 and its central star.

4. MOLECULAR AND IONIZED MATERIAL DISTRIBUTION

In order to make a fair comparison of the distribution of the molecular and ionized material in these PNe, their [N II] and H α +[N II] optical images from M96 were rebinned to the same pixel scale of the near-IR images ($0.64''$ pixel⁻¹). A gaussian filter was used to degrade

the optical images and make the FWHM of point sources in the field similar for both sets of images (1''1–1''5). The contour plot of H₂ emission has been overlaid over a gray-scale representation of the [N II] images in Fig. 1 [*bottom*].

Most of the H₂ morphological features closely trace the corresponding [N II] optical features. The bright condensations observed in the rings in H₂ are also found in the [N II] images. Furthermore, the optical design of the lobes in [N II] is also outlined in H₂. The H₂ emission in the bipolar lobes is relatively enhanced compared to the optical [N II] lines. The f_{LR} ratios given in Table 2 are in the range 0.2–0.4; the corresponding ratios in the [N II] lines are ~ 5 times smaller.

We extracted spatial profiles from the H₂ and [N II] images to quantify the dimensions of the molecular and low-ionization material distributions. The spatial line profiles, extracted along representative directions of the nebulae, are shown in Figure 3. They have been used to measure the size of well defined features in both the H₂ and [N II] images. In particular, the size of the rings measured from peak to peak are listed in Table 3. Given the pixel size and the expected FWHM for a point sources, the position is accurate within 0''1–0''2. The H₂ emission from the ring closely embraces the [N II] optical emission in the H₂ dominated bipolar PNe. Differences in size goes from 0''6 to 3''9. Furthermore, emission in the H₂ extends further than in the [N II] line. When lobes are mapped, they appear to be more prominent in the H₂ line (*e. g.* K 4-55, or M 1-75), partly due to the enhancement of H₂ emission from the lobes described above. A singular case is the H₂ emission detected in the lobes of NGC 6881 described in §3.3. In this case, we measured the lobes width at two different slit positions.

Now, it would be desirable to transform the angular differences in size to linear sizes. However, the use of statistical distances is uncertain in these objects, since its particular morphology makes the spherical symmetry assumption on which those methods are based unreasonable (Pottasch 1984; Maciel 1997). As there are no individual distance estimates for most of these objects, we have adopted the averaged value among those included in Acker et al. (1992), and the more recent estimations given by Van de Steene & Zijlstra (1994), and Zhang (1995). Using these averaged distances, as given in Table 3, the thickness of the region located between the [N II] emission peak and the H₂ peak (column 7) result to be in a narrow range from 7×10^{15} to 6.4×10^{16} cm. Thus, the H₂ emission occurs in a narrow region just outside the ionized zone.

5. DISCUSSION

We have searched for molecular hydrogen emission in a sample of 15 bipolar PNe. The high detection rate ($\sim 90\%$) found in our sample is the result of its bias to

bipolar morphologies, since the frequency of detections in a morphologically unbiased sample of PNe (*e. g.* Kastner et al. 1996) is rather small, $\sim 40\%$. Moreover, almost 70% of the combined sample of bipolar PNe surveyed by Kastner et al. (1996) and this work exhibit H₂ emission. These numbers support the idea that bipolar PNe are, at least partially, ionization-bounded, with important reservoirs of molecular material, and that they offer suitable physical conditions for the excitation of H₂.

The H₂ emission closely traces the [N II] ionized emission in most of the PNe in our sample. This behavior has been reported, although based on mostly ‘qualitative’ arguments (Kastner et al. 1996), data of poor (5''–10'') spatial resolution (Beckwith, Persson, & Gatley 1978; Webster et al. 1988), or the quantitative analysis of a few large PNe, as it is the case of the elliptical PN NGC 6720 (Zuckerman & Gatley 1988). The improved spatial resolution ($\sim 1''$) of our narrow-band [N II] and H₂ images has enabled us to make a detailed analysis of the relative distribution of the ionized and H₂ molecular emission in eight bipolar PNe. The H₂ emission is found in a thin shell (≤ 0.1 times the optical size), just outside the ionized [N II] zone both in the rings and the walls of the lobes. As pointed out by Kastner et al. (1996), the H₂ emission is brightest toward the ring of the nebula. Moreover, our data reveal that the H₂ emission is enhanced in the lobes in comparison to the [N II] optical emission.

One of the main results derived from this work is that a firm connection can now be established between the detailed nebular morphology of bipolar PNe and the H₂ intensities and H₂/Br γ flux ratios observed. The PNe with Br morphology show larger H₂ to Br γ flux ratios, as well as larger H₂ intensities. In contrast, B PNe have the smallest H₂ to Br γ flux ratios and H₂ intensities. This result strengthens the earlier suggestion by Webster et al. (1988) that strong H₂ emission is found almost exclusively among Br PNe. Adding Webster et al.’s sample to ours, we find that $\sim 80\%$ of the Br PNe surveyed belong to the group with strong H₂ intensities.

Why is H₂ intensity enhanced in Br PNe? In order to assess and clarify the underlying physics of this correlation, several hypotheses have been considered, although all of them have their own share of difficulties. Moreover, they do not exclude each other.

“*B and Br PNe are at different evolutionary stages*”.— This idea, originally proposed by Balick (1987), is supported by the different physical properties of B and Br PNe described in §3.1 and §3.2. The Br PNe smaller densities and larger sizes suggest larger dynamical ages. Indeed, the high surface brightness of the ring of Br PNe requires a long time in order to allow the fast wind from the central star to have swept up over the ring the material that once was inside it. To this effect, the fact that the central stars of Br PNe are faint is consistent with an evolved stage.

The H_2 to $Br\gamma$ ratio is expected to increase with time for PNe from massive progenitors (Natta & Hollenbach 1998). According to this model, the predicted ratios increase from ~ 0.1 for young PNe to ~ 10 for old PNe, in reasonable agreement with the observed ratios. However, Bobrowsky & Zipoy (1989) and Natta & Hollenbach (1998) models predict a steep decrease of the H_2 intensity with time. For massive progenitors ($0.696 M_\odot < M_{\text{core}} < 0.836 M_\odot$) with a high density molecular shell ($\geq 10^5 \text{ cm}^{-3}$), Natta & Hollenbach's model predicts the decline of the H_2 intensity by a factor > 100 in the early nebular evolution. The agreement between the theoretical predictions and the increase of H_2 intensity with time is possible if a lower initial density of the molecular envelope ($\leq 10^4 \text{ cm}^{-3}$) is assumed. In this case, it has been shown (Vicini et al. 1999) that the intensity of the H_2 $2.122 \mu\text{m}$ line does not decline for a PN with core mass $0.7 M_\odot$ as it evolves, but it is enhanced (the reader is referred to this paper for further details). If the detailed bipolar morphology is indeed related to the evolution of bipolar PNe, the bulk of observational data presented by Webster et al. (1988) and this paper indicate that low initial densities of the molecular envelopes are the rule rather than the exception in bipolar PNe.

“The H_2 emission in B and Br PNe have different prevalent excitation mechanisms”.— Note that this does not necessarily exclude the previous evolutionary hypothesis, as the prevalent excitation mechanism may be different as the PN evolves.

Shocks may play a significant role in the excitation of molecular hydrogen in bipolar PNe. According to Natta & Hollenbach (1998), the shock contribution to the intensity of the H_2 $2.122 \mu\text{m}$ line is expected to be

$$\sim 0.1 \times \dot{M}_{\text{RG}} f_{\text{RG}} / 10^{-5} M_\odot \text{ yr}^{-1} \quad (2)$$

over most of the PN lifetime, where \dot{M}_{RG} and f_{RG} are the mass-loss rate and filling factor of the red giant wind. Therefore, for high mass-loss rates and/or non-isotropic red giant winds, shock excitation would dominate the H_2 excitation. Indeed, the H_2 $2.122 \mu\text{m}$ peak intensities predicted by shock models (Draine, Roberge, & Dalgarno 1983; Burton et al. 1992) for the typical expansion velocities ($30-100 \text{ km s}^{-1}$) of bipolar PNe (Corradi & Schwarz 1995) are in agreement with the observed peak intensities in our sample ($1.2-5.3 \times 10^{-4} \text{ erg cm}^{-2} \text{ s}^{-1} \text{ sr}^{-1}$).

However, no evidence for shock excitation is found in the archetypical Br PN NGC 2346. The prevalent H_2 excitation mechanism in this PN has been shown to be UV excitation (Hora et al. 1999; Vicini et al. 1999). It can be argued that even with this evidence, the shock excitation cannot easily be disregarded, as the presence of fast winds and dissociating shocks are able to produce UV photons in the shocked wind which would indirectly excite the H_2 .

On the other hand, even if shock excitation is important in bipolar PNe, it is not clear why H_2 intensity should

be enhanced in Br PNe and not in B PNe. Both subsamples of nebulae exhibit the same kinematical properties: the expansion velocity of the lobes of these bipolar PNe ranges from 30 to 100 km s^{-1} , whereas rings expand more slowly, at $5-25 \text{ km s}^{-1}$ (Guerrero & Manchado, unpublished data). Alternatively, the H_2 line intensities may strongly depend on the density of the material and on the shock structure (Shull & Hollenbach 1978; Burton et al. 1992), so that the characteristic geometry of Br PNe would favor the enhancement of the H_2 emission.

An additional excitation mechanism that must be taken into account in the late evolution of the PN is the presence of X-rays from the hot central star. Natta & Hollenbach (1998), and Vicini et al. (1999) have highlighted the importance of the X-ray heating in enhancing the predicted H_2 intensity, specially for PNe with low initial densities of the molecular envelope. However, the uncertainty in the far UV and soft X-ray spectrum of PNe forces to use this result with special caveat. No X-ray emission has been detected in bipolar PNe up to now, most likely because of the high extinction and low luminosity of the central stars of bipolar PNe (Guerrero, Chu, & Gruendl 1999).

Obviously, a detailed spatially-resolved spectroscopic analysis of the H_2 emission line spectrum in a large sample of bipolar PNe is needed to fully address these issues.

“B and Br PNe proceed from different evolutionary tracks”.— If Br PNe follow a different evolutionary track with enhanced mass-loss rates on the AGB, they would have much more massive molecular envelopes than B PNe. Subsequently, the H_2 emission in Br PNe would be stronger than in B PNe. The evolution from more massive stars than the progenitors of B PNe or from a binary system undergoing a common envelope phase may be the cause for the enhanced mass-loss rate in Br PNe. The lack of observational evidence to support these particular evolutionary tracks for B and Br PNe would make it a highly speculative conclusion.

6. CONCLUSIONS

We have presented continuum-subtracted flux-calibrated H_2 and $Br\gamma$ images of a sample of 15 bipolar PNe. The high H_2 detection rate within this sample strengthens the idea that bipolar PNe are molecular rich objects where H_2 finds suitable physical conditions for its excitation.

The H_2 intensity and H_2 to $Br\gamma$ flux ratio are found to change with the detailed morphology of the bipolar PNe; PNe with Br morphology exhibit the highest H_2 to $Br\gamma$ flux ratios, and H_2 absolute fluxes. Although we cannot discard the possibility of B and Br PNe proceeding from different evolutionary tracks, most observational data indicate that the observed correlation reflects the fact that B and Br PNe are in a different evolutionary stage. In order to explain the enhancement of the H_2 intensity with time, the initial density of the molecular envelope must be low.

The different H₂ intensities and H₂ to Br γ flux ratios observed in each of these two subgroups of bipolar PNe may also be connected to different prevalent excitation mechanisms, which can, at the same time, be a consequence of the different evolutionary stage.

The H₂ emission from H₂-dominated bipolar PNe is mainly located in the ring, although fainter H₂ emission is also found in the lobes. The comparison between H₂ and [N II] images of these PNe reveals that the H₂ emission is distributed in a narrow region just outside the ionized material and that it is more enhanced in the lobes compared to the ionized [N II] emission.

The 2.2m telescope at the German-Spanish Astronomical Centre, Calar Alto, is operated by the Max-Planck-Institut für Astronomie, Heidelberg, jointly with the Spanish National Comission for Astronomy. This research was partially funded through grant PB94-1274 from the Dirección General de Investigación Científica y Técnica of the Spanish Ministerio de Educación y Ciencia. MAG is supported partially by the Dirección General de Enseñanza Superior e Investigación Científica of the Spanish Ministerio de Educación y Cultura.

REFERENCES

Acker, A., Marcout, J., Ochsenbein, F., Stenholm, B., Tylenda, R., & Schohn, C. 1992, in The Strasbourg-ESO Catalogue of Galactic Planetary Nebulae, Part II (Garching: European Southern Observatory)

Acker, A., Stenholm, B., Tylenda, R., & Raytchev, B. 1991, A&AS 90, 89

Balick, B. 1987, AJ, 94, 671

Beckwith, S., Persson, S. E., & Gatley, I. 1978, ApJ219, L33

Black, J. H., & van Dishoeck, E. F. 1987, ApJ322, 412

Bobrowsky, M., & Zipoy, D. M. 1989, ApJ347, 307

Burton, M. G., Hollenbach, D. J., & Tielens, A. G. G. M. 1992, ApJ, 399, 563

Casali, M. M., & Hawarden, T. G., 1992, JCMT-UKIRT Newsletter, 3, 33

Corradi, R. L. M., & Schwarz, H. E. 1995, A&A, 293, 871

Cox, P., Maillard, J.-P., Huggins, P. J., Forveille, T., Simons, D., Guilloteau, S., Rigaut, F., Bachiller, R., & Omont, A. 1997, A&A321, 907

Dinerstein, H. L. 1991, PASP, 103, 861

Draine, B. T., Roberge, W. G., & Dalgarno, A. 1983, ApJ, 264, 485

Guerrero, M. A., & Manchado, A. 1998, ApJ, 508, 262

Guerrero, M. A., Chu, Y.-H., & Gruendl, R. A. 1999, AAS, 194, 85.14

Hora, J. L., & Latter, W. B. 1996, AAS, 189, 97.08

Hora, J. L., Latter, W. B., & Deutsch, L. K. 1999, ApJ, in press

Huggins, P. J., Bachiller, R., Cox, P., & Forveille, T. 1996, A&A, 315, 284

Huggins, P. J., & Healy, A. P. 1989, ApJ, 346, 201

Josselin, E., Bachiller, R., Manchado, A., & Guerrero, M. A. 1999, submitted to A&A

Kaler, J. B., Chu, Y.-H., & Jacoby, G. H. 1988, AJ, 96, 1407

Kastner, J. H., Gatley, I., Merrill, K. M., Probst, R. G., & Weintraub, D. 1994, ApJ, 421, 600

Kastner, J. H., Weintraub, D., Gatley, I., Merrill, K. M., & Probst, R. G. 1996, ApJ, 462, 777

Latter, W. B., & Hora, J. L. 1997, in Planetary Nebulae, IAU Symp. 180, eds. H. J. Habing & H. J. G. L. M. Lamers (Kluwer: Dordrecht), 254

Latter, W. B., Kelly, D. M., Hora, J. L., & Deutsch, L. K. 1995, ApJS, 100, 159

Maciel, W. J. 1997, in Planetary Nebulae, IAU Symp. 180, eds. H. J. Habing & H. J. G. L. M. Lamers (Kluwer: Dordrecht), 49

Manchado, A. 1997, in Planetary Nebulae, IAU Symp. 180, eds. H. J. Habing & H. J. G. L. M. Lamers (Kluwer: Dordrecht), p. 24

Manchado, A., Guerrero, M. A., Stanghellini, L., & Serra-Ricart, M. 1996, The IAC Morphological Catalog of Northern Galactic Planetary Nebulae, IAC, La Laguna (M96)

Natta, A., & Hollenbach, D. 1998, A&A, 337, 517

Osterbrock, D. E. 1989, Astrophysics of Gaseous Nebulae and Active Galactic Nuclei, University Science Books: Mill Valley

Peimbert, M., & Torres-Peimbert, S. 1983, in Planetary Nebulae, IAU Symp. 103, ed. D. R. Flower (Reidel: Dordrecht), p. 233

Pottasch, S. R. 1984, Planetary nebulae, a study of late stages of stellar evolution (Reidel: Dordrecht), p. 114

Shull, J. M., & Hollenbach, D. J. 1978, ApJ, 220, 525

Shupe, D. L., Armus, L., Matthews, K., & Soifer, B. T. 1995, AJ, 109, 1173

Sternberg, A., & Dalgarno, A. 1989, ApJ, 338, 197

Tielens, A. G. G. M. 1993, in Planetary Nebulae, IAU Symp. 155, eds. R. Weinberger & A. Acker (Kluwer: Dordrecht), 155

Treffers, R. T., Fink, U. F., Larson, H. L., & Gautier, N. T. 1976, ApJ, 209, 793

Van de Steene, G. C., & Zilstra, A. A. 1994, A&AS 108, 485

Vicini, B., Natta, A., Marconi, A., Testi, L., Hollenbach, D., & Draine, B. T. 1999, A&A, 342, 823

Webster, B. L., Payne, P. W., Storey, J. W. V., & Dopita, M. A. 1988, MNRAS 235, 533

Zhang, C. Y. 1995, ApJS, 98, 659

Zuckerman, B., & Gatley, I. 1988, ApJ, 324, 501

TABLE 1
FILTER DESCRIPTION

Filter name	Central wavelength [μm]	FWHM [μm]
H_2 S(1) 1–0	2.122	0.021
$\text{Br}\gamma$	2.166	0.022
K'	2.100	0.340

TABLE 2
PROPERTIES OF THE BIPOLAR PLANETARY NEBULA SAMPLE

Object	PN G	Morph. class ¹	PN size ¹ [arcsec]	Ring size ¹ [arcsec]	$F(\text{H}\beta)$ ² [10^{-14} erg cm ⁻² s ⁻¹]	$F(\text{H}_2)$ [10^{-14} erg cm ⁻² s ⁻¹]	$F(\text{Br}\gamma)$ [10^{-14} erg cm ⁻² s ⁻¹]	$\frac{F(\text{H}_2)}{F(\text{Br}\gamma)}$	f_{LR}
M 1-57	022.1–02.4	B	24.3	10.6	4100	21	239	0.1	0.14
M 1-59	023.9–02.3	Br	24.2	8.9	5100	61	320	0.2	0.22
M 2-46	024.8–02.7	Q	30.0	7.0	830	11	64	0.2	...
PC 20	031.7+01.7	Br	11.8	6.5	...	53	90	0.6	0.75
M 4-14	043.0–03.0	Q	27	8.5	720	192	18	10.8	0.30
He 2-428	049.4+02.4	Br	63	18	56	...	43
K 3-34	059.0+04.6	Br	20.8	10.5	32	47	0.37
He 2-437	061.3+03.6	B	45	4.6	780	12	115	0.1	...
M 1-75	068.8–00.0	Br	11.8	6.5	230	389	68	5.7	0.38
K 3-58	069.6–03.9	Br	23	12.7	150	227	7.2	32.0	0.20
NGC 6881	074.5+02.1	Q	29.5	5.0	2700	125	243	0.5	0.19
M 4-17	079.6+05.8	Br	24	20	230	324	30	10.7	0.28
K 4-55	084.2+01.1	Br	71	9.0	120	245	17	14.0	0.29
M 2-52	103.7+00.4	Br	60	23	3800	198	23	8.6	0.18
BV 1	119.3+00.3	Br	48	7	280	197

REFERENCES.—(1) Manchado et al 1996; (2) Acker et al 1992

TABLE 3
COMPARISON OF THE H₂ AND [N II] SPATIAL DISTRIBUTIONS

Object	Position angle [deg]	H ₂ size [arcsec]	[N II] size [arcsec]	Relative size H ₂ /[N II]	Distance [kpc]	Thickness [10 ¹⁶ cm]
M 1-59	40	3.2	3.2	1.00	3.0	< 0.3
M 4-14	140	6.4	5.8	1.11	5.2	2.3
M 1-75	54	9.6	8.3	1.15	3.4	3.3
	135	17.9	16.6	1.08		3.3
K 3-58	8	8.3	7.0	1.18	6.1	5.9
NGC 6881	45 ^a	9.6	4.5	2.14	3.1	11.8
	45 ^b	11.5	4.0 ^c	2.90		17.4
M 4-17	27	20.5	16.6	1.23	2.2	6.4
K 4-55	4	7.7	7.0	1.09	1.4	0.7
	80	10.9	9.0	1.21		1.8
M 2-52	62	7.0	7.0	1.00	3.3	< 0.3
	120	11.5	10.9	1.06		1.5

^aOffset of 10 arcsec to the south-east.

^bOffset of 10 arcsec to the north-west.

^cFWHM of the line profile.

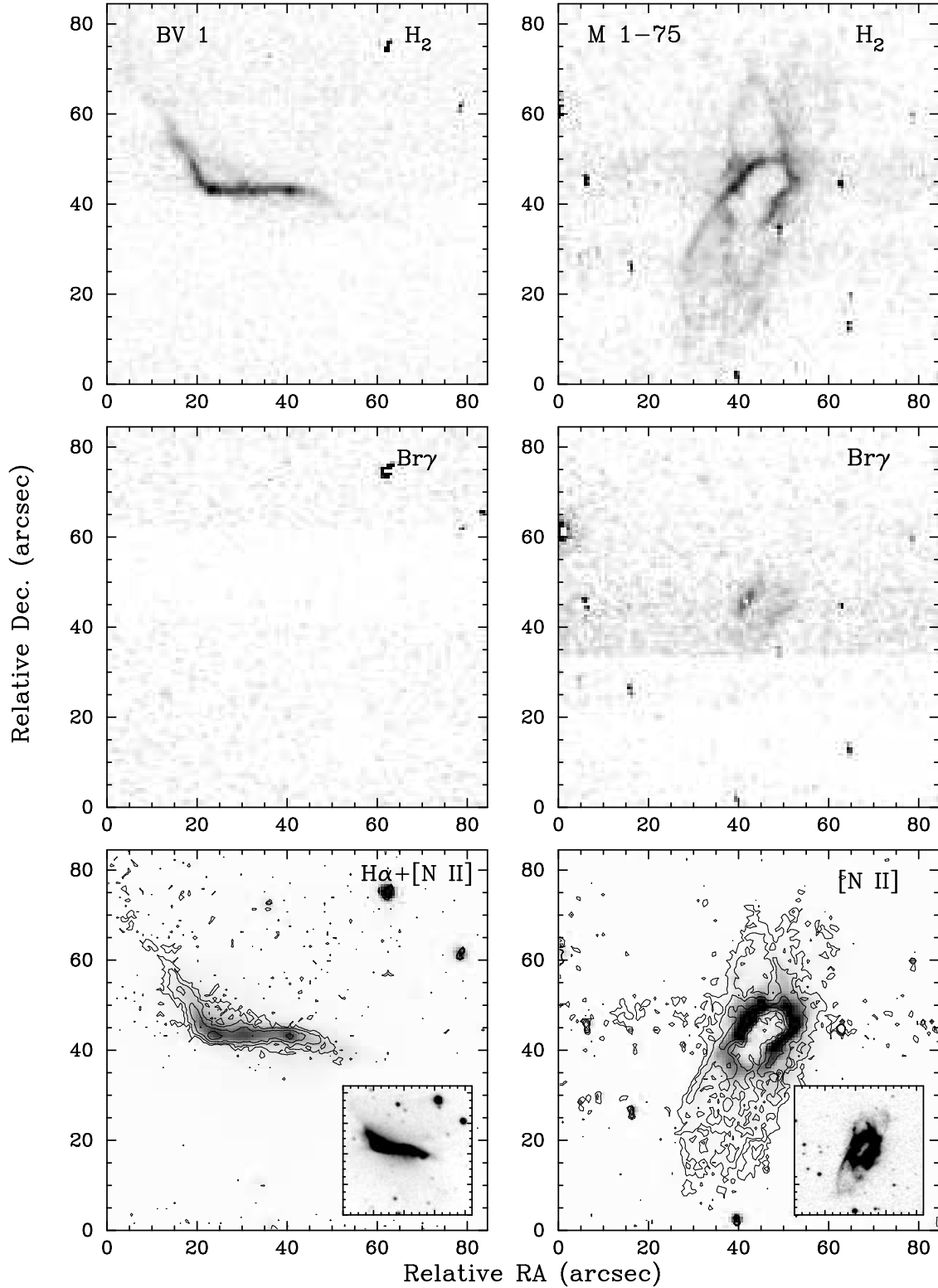


FIG. 1a— Gray-scale representation of the H_2 (top), and $\text{Br}\gamma$ (center) continuum-subtracted images, and of the $[\text{N II}]$ emission line image (bottom) from the Manchado et al.'s catalog of BV 1 (left), and M 1-75 (right). Contour plot of the $2.122 \mu\text{m}$ H_2 emission is overlaid on the $[\text{N II}]$ image whose intensity levels have been set up to allow a fair comparison with the molecular emission. The lowest contour is at 3σ . The insets at the corners of the $[\text{N II}]$ images are displayed at low intensity levels to emphasize the fainter regions of the nebula. The image scale is the same for all the images of each nebula. North is top, east is left.

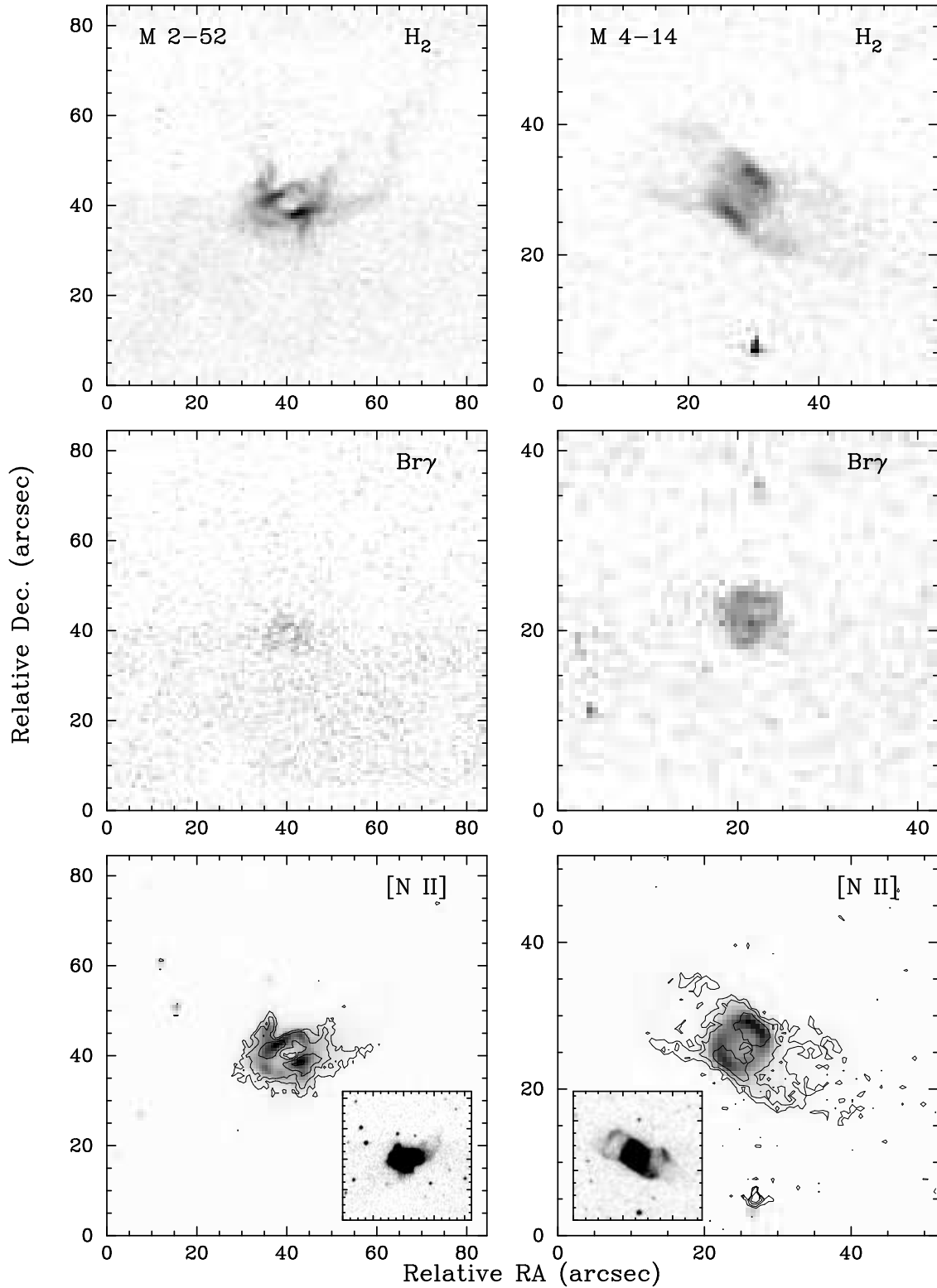


FIG. 1b—Same as Fig. 1a, but for M 2-52 (left), and M 4-14 (right).

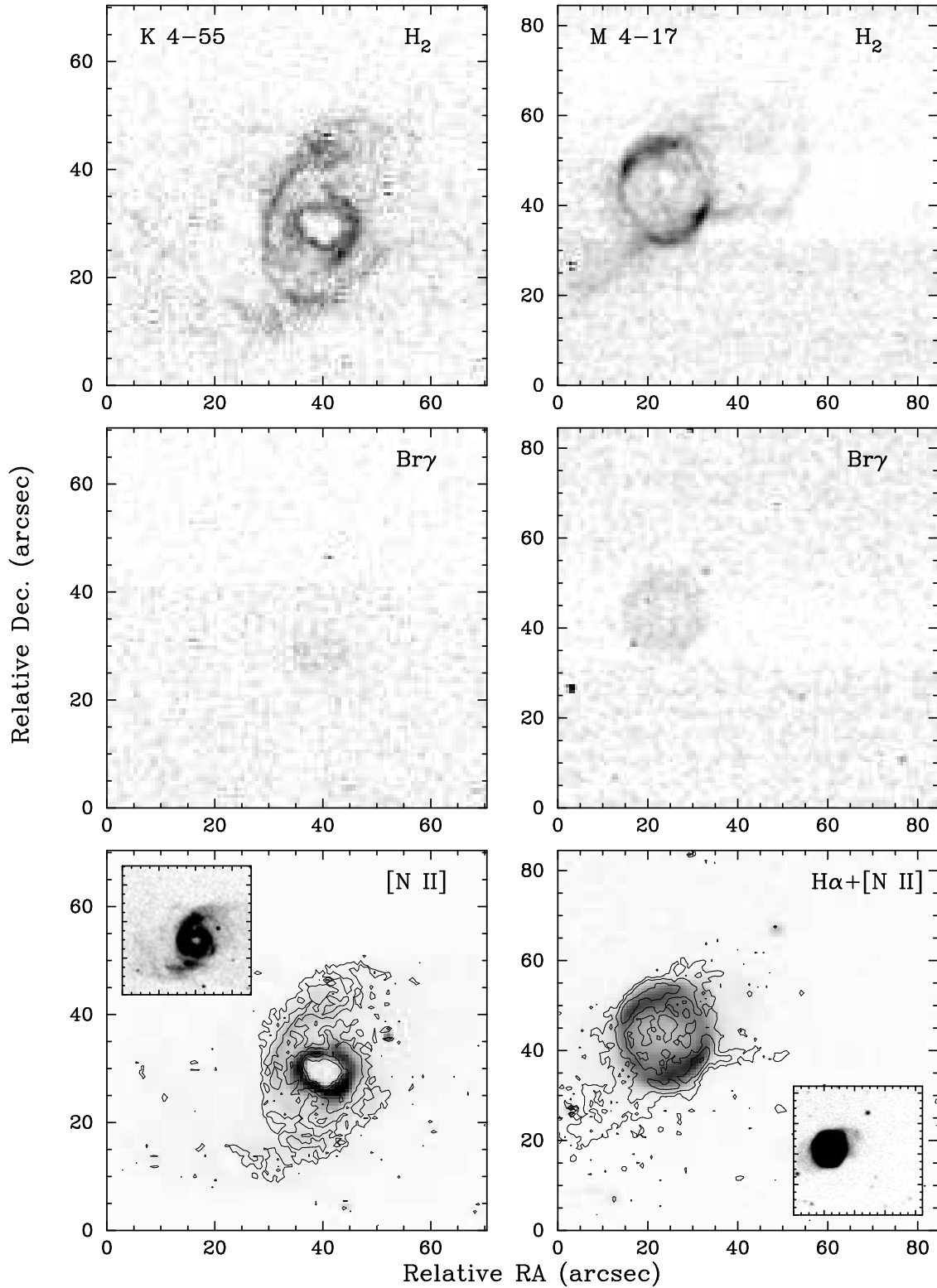


FIG. 1c— Same as Fig. 1a, but for K 4-55 (left), and M 4-17 (right).

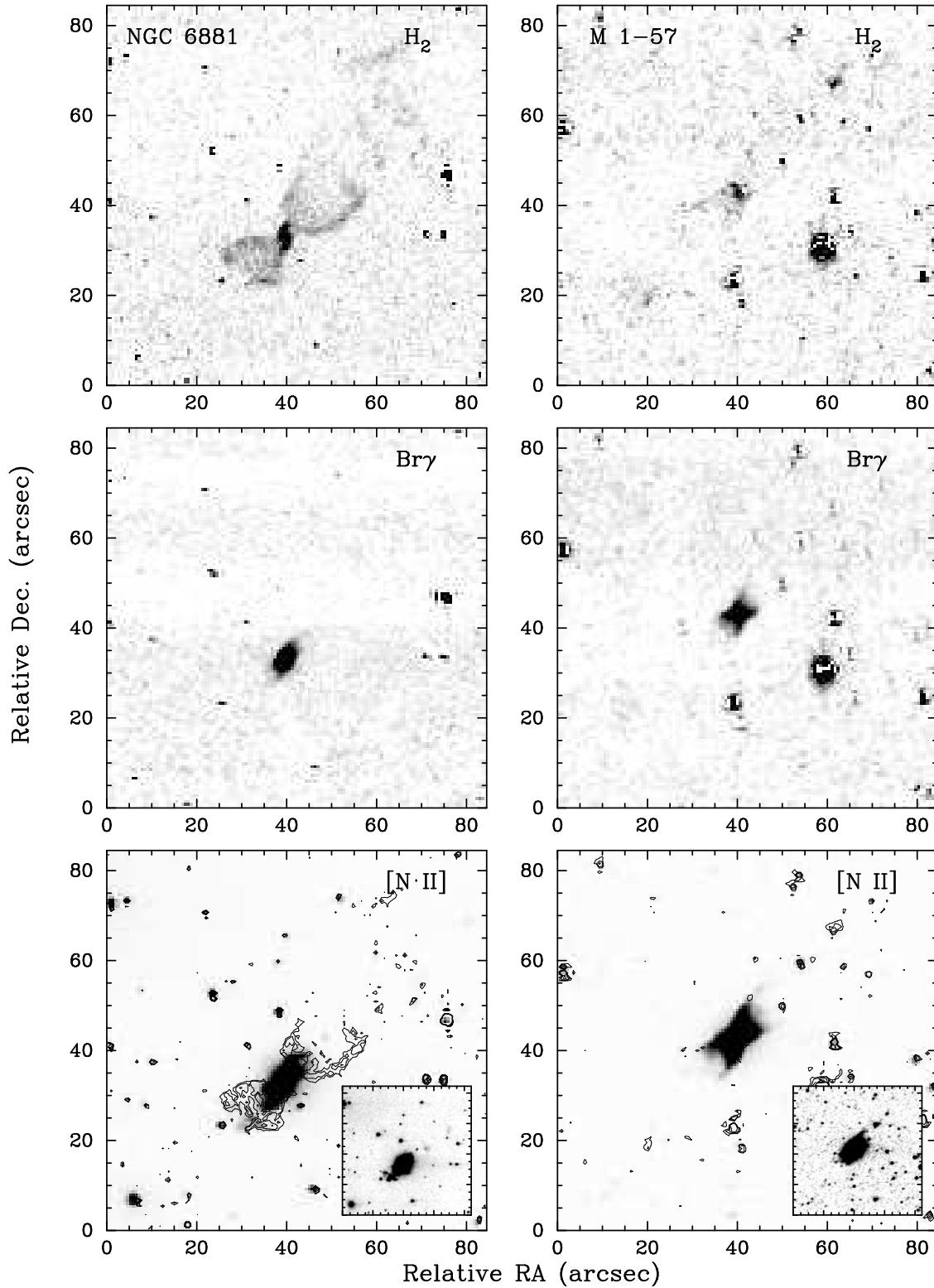


FIG. 1d— Same as Fig. 1a, but for NGC 6881 (left), and M 1-57 (right).

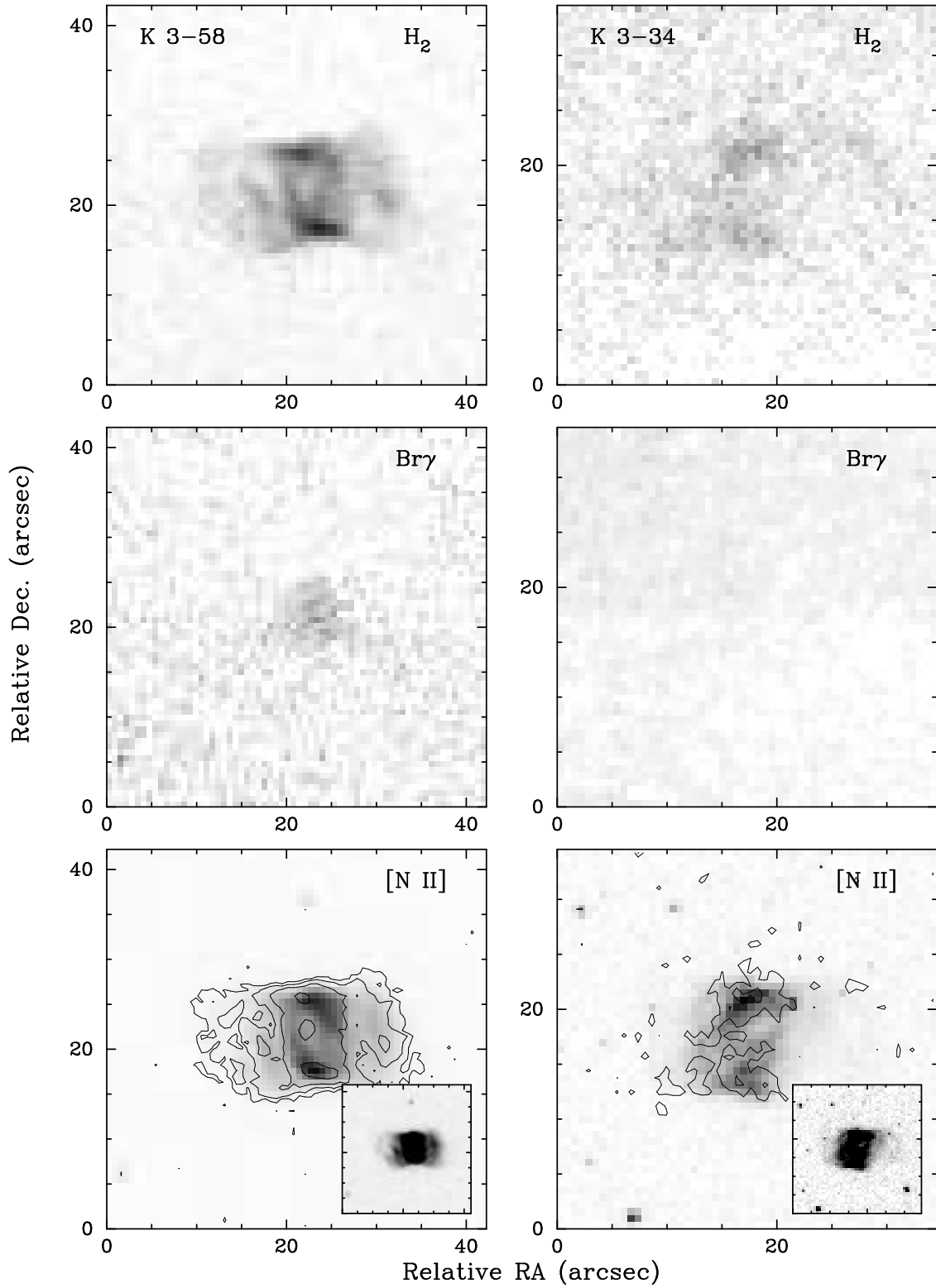


FIG. 1e— Same as Fig. 1a, but for K 3-58 (left), and K 3-34 (right).

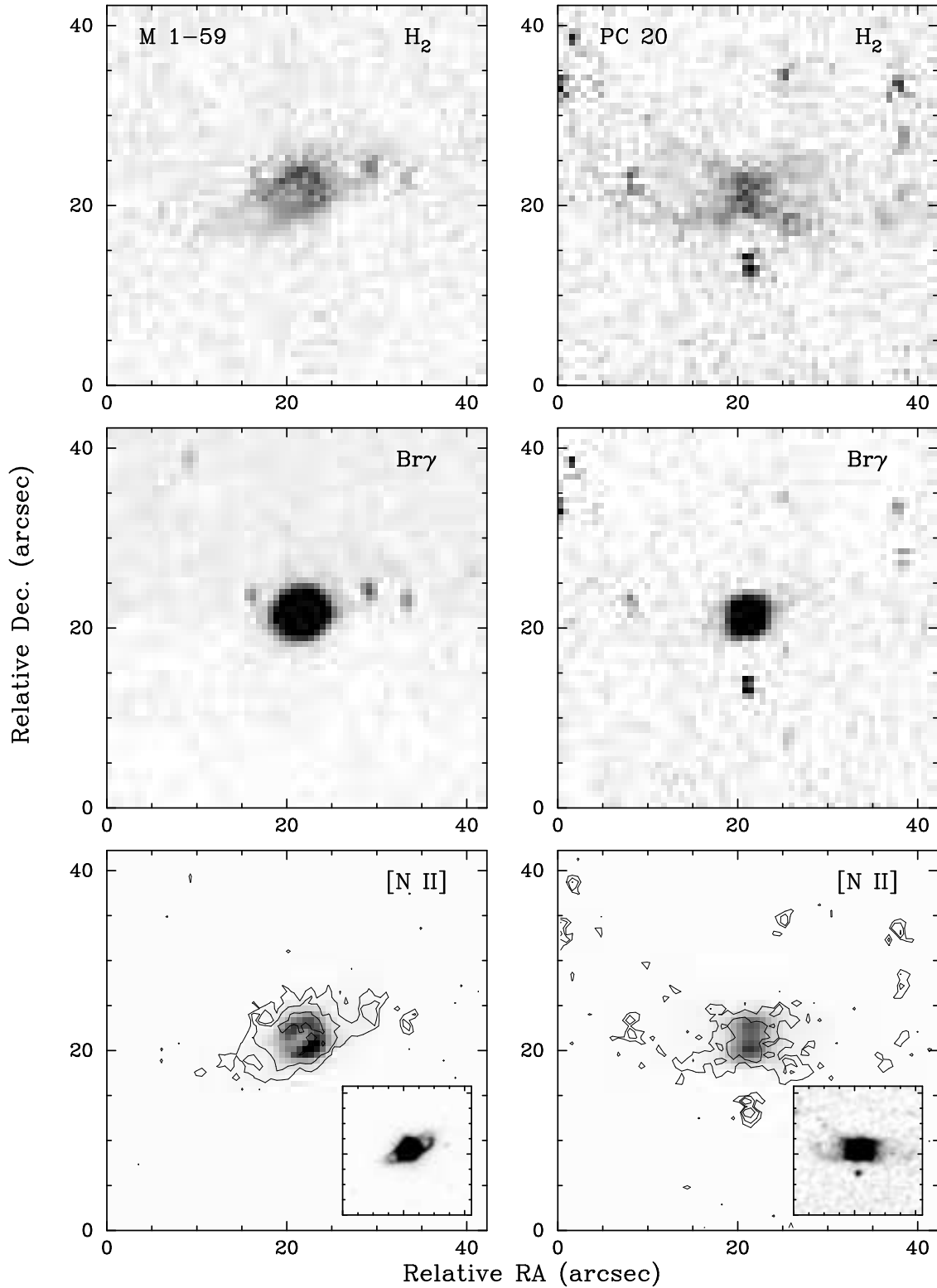


FIG. 1f— Same as Fig. 1a, but for M 1-59 (left), and PC 20 (right).

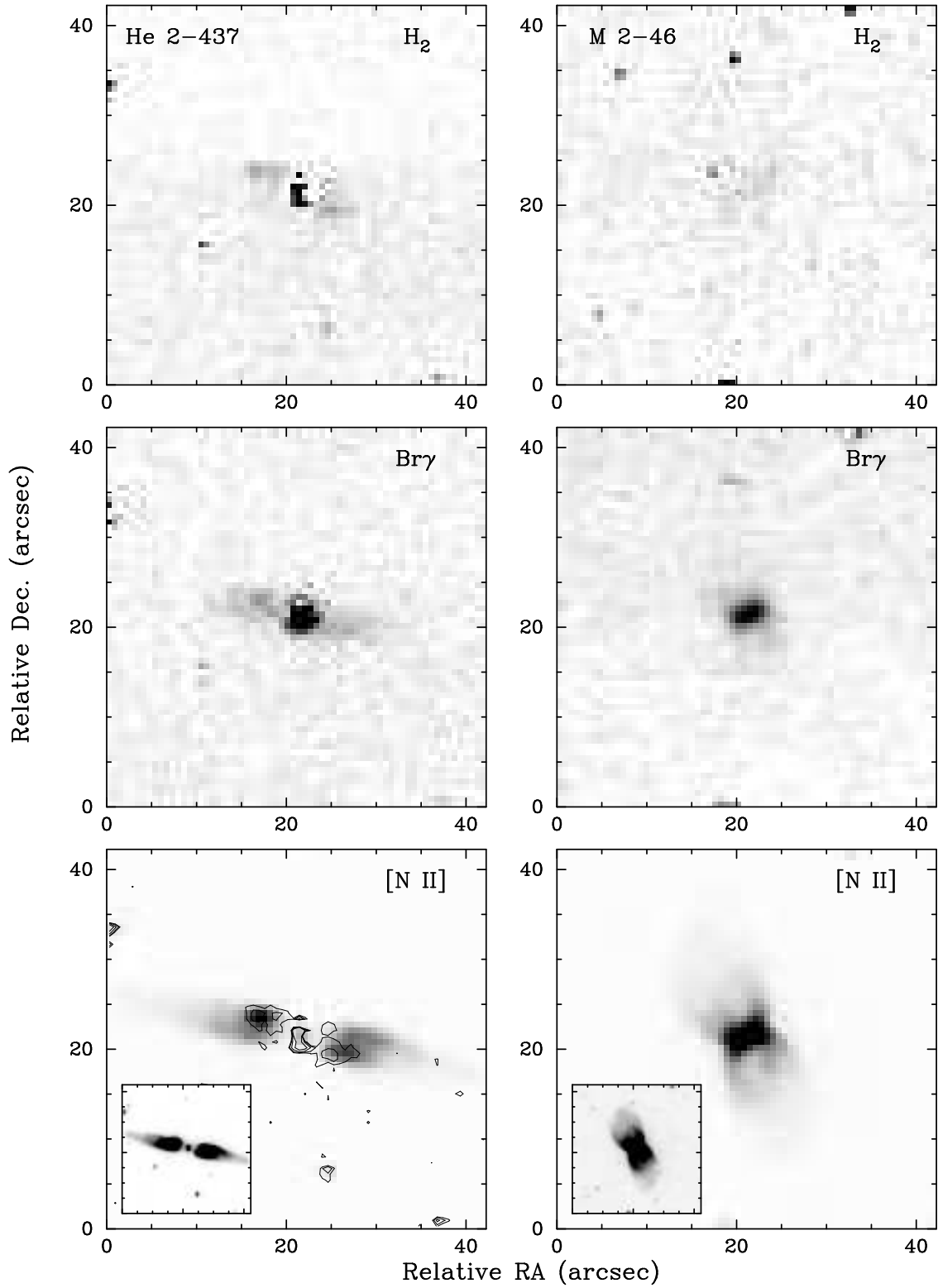


FIG. 1g— Same as Fig. 1a, but for He 2-437 (left), and M 2-46 (right).

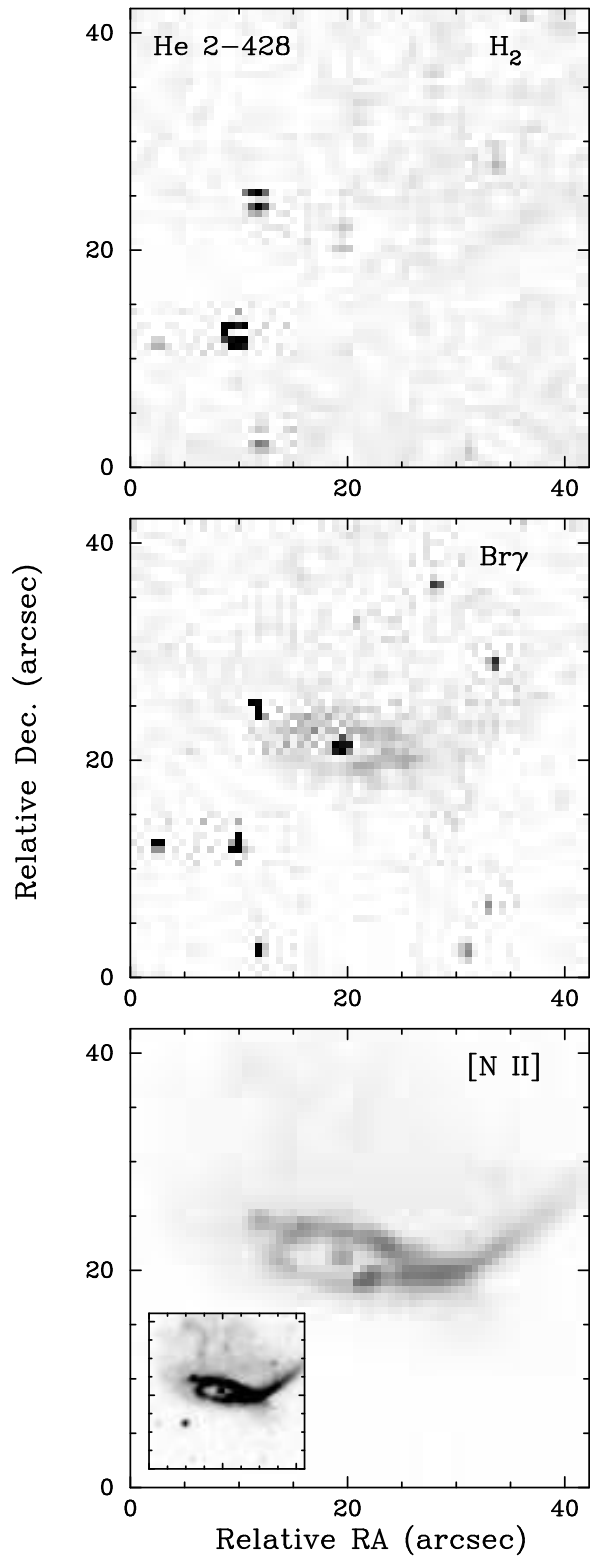


FIG. 1h— Same as Fig. 1a, but for He 2-428.

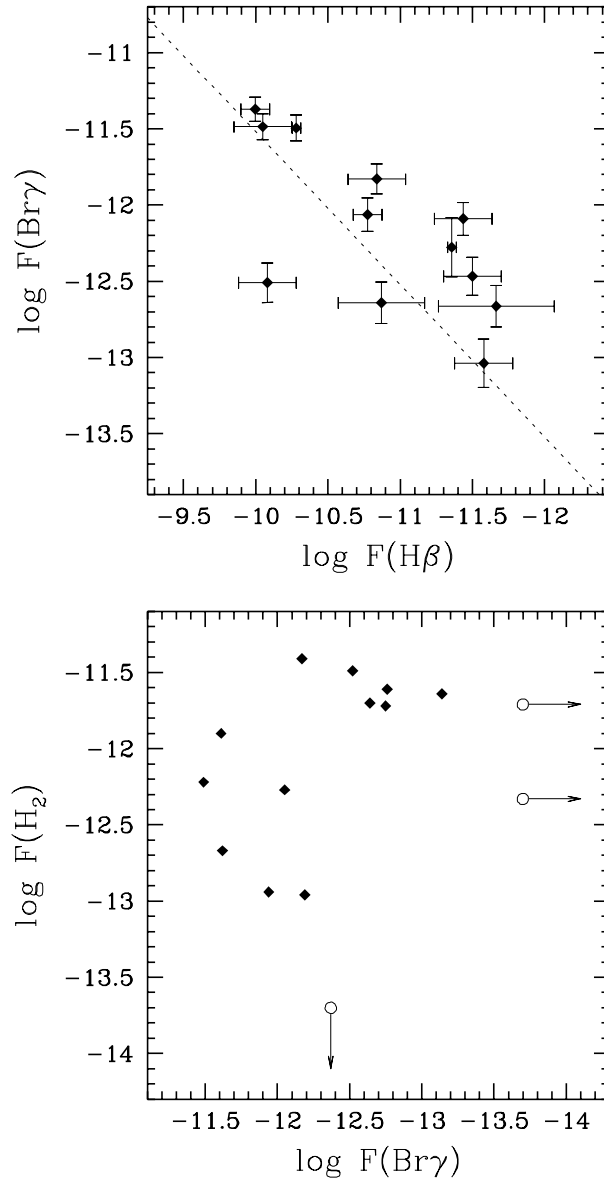


FIG. 2—(top) The Br γ fluxes plotted against the H β fluxes as given by Acker et al. (1992). The fluxes have been corrected of interstellar extinction using the standard extinction law from Pottasch (1984), and the H β extinction coefficients computed from the comparison of the H α to H β flux ratio given in Acker (1992) and the theoretical Balmer decrement (Osterbrock 1989). The errorbar associated to the Br γ and H β fluxes have been plotted, as well as the predicted theoretical ratio (dashed line). (bottom) The measured H $_2$ fluxes plotted against the Br γ fluxes. When no detection was made, an upper limit of the flux is given and indicated by an open dot. The sample appears separated in two regions of this diagram characterized by stronger H $_2$ or Br γ fluxes.

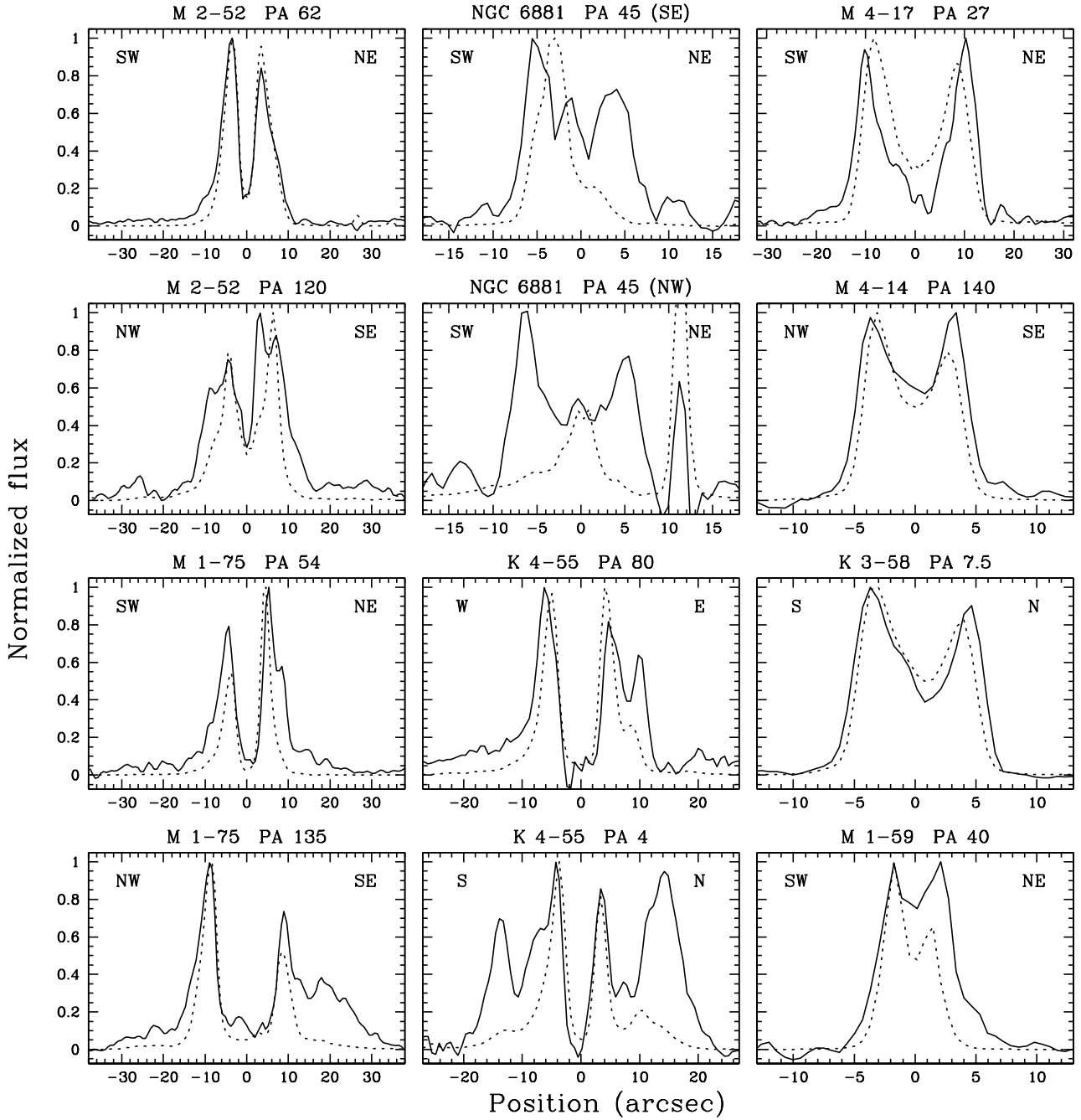


FIG. 3— Spatial profiles extracted along selected directions comparing the 2.122 μ m H₂ (solid line) and [N II] optical (dashed line) emission. The position angle and orientations are indicated on each panel.